Characterisation of tau PET tracer [^{18}F]AV-1451 binding to *post-mortem* tissue in Alzheimer's disease, primary tauopathies and other dementias

Kerstin Sander[a,#], Tammaryn Lashley[b,#], Priya Gami[b], Thibault Gendron[a], Mark F Lythgoe[c], Jonathan D Rohrer[d], Jonathan M Schott[d], Tamas Revesz[b], Nick C Fox[d,#] and Erik Årstad[a,#,*]

[a] Institute of Nuclear Medicine and Department of Chemistry, University College London, 235 Euston Road (T-5), London NW1 2BU, UK

[b] Institute of Neurology, Queen Square Brain Bank, University College London, 1 Wakefield Street, London WC1N 1PJ, UK

[c] Centre for Advanced Biomedical Imaging, University College London, 72 Huntley Street, London WC1E 6DD, UK

[d] Institute of Neurology, Dementia Research Centre, University College London, 8–11 Queen Square, London WC1N 3BG, UK

[#] KS and TL contributed equally to the research, and NCF and EÅ are joint senior authors of this paper.

[*] Corresponding author (email: e.arstad@ucl.ac.uk; phone/fax: +44 20 7679 2344)

Abstract

INTRODUCTION: Aggregation of tau is a hallmark of many neurodegenerative diseases, and tau imaging with positron emission tomography (PET) may allow early diagnosis and treatment monitoring. We assessed binding of the PET tracer [^{18}F]AV-1451 in a range of dementias.

METHODS: Phosphorimaging was used to quantify binding to *post-mortem* brain tissue from 33 patients with different, histopathologically characterised, neurodegenerative dementias.

RESULTS: [^{18}F]AV-1451 showed high specific binding in cases with Alzheimer's disease (AD), moderate binding in Pick's disease and frontotemporal dementia with parkinsonism-17, and low but displaceable binding in corticobasal degeneration, progressive supranuclear palsy, non-tau proteinopathies and in controls without pathology. Tracer binding did not correlate with tau load within disease groups.

DISCUSSION: [^{18}F]AV-1451 binds to tau in AD, and some other tauopathies. However, evidence for a non-tau binding site and lack of correlation between tracer binding and antibody staining, suggest that reliable quantification of tau load with this tracer is problematic.

Keywords

Dementia, tau, neurodegeneration, PET, [^{18}F]AV-1451, phosphorimaging, immunohistochemistry

Abbreviations for neurodegenerative diseases

AD, Alzheimer's disease; CBD, corticobasal degeneration; DLB/PDD, dementia with Lewy bodies/Parkinson's disease with dementia; FTLD-TDPA/C, frontotemporal lobar degeneration linked to TAR DNA-binding protein-43, type A/C; FTDP-17, frontotemporal dementia with parkinsonism linked to chromosome 17 (caused by a mutation of the microtubule-associated protein tau (MAPT) gene); PICK, Pick's disease; PSP, progressive supranuclear palsy

1. Background

The accumulation of misfolded proteins in the central nervous system (CNS) is a characteristic, often defining, feature of neurodegenerative diseases. Pathological aggregation of tau protein occurs in a number of diseases causing dementia and/or movement disorders [1]. For instance, tau inclusions are found in Alzheimer's disease (AD), the most common tauopathy, which accounts for 50–70% of dementia cases, and in some forms of frontotemporal lobar degeneration (FTLD; 10–20% of dementia cases) – in these disorders the tau inclusions are a hallmark of the disease [2–4]. Depending on whether the tau filaments are formed primarily by tau isoforms with three or four tandem repeats in their microtubule binding domain (3R-tau or 4R-tau), or a mixture of 3R-tau and 4R-tau, the tau aggregates define different neurodegenerative disease phenotypes associated with tau malfunctioning [1,5,6]. In patients with AD, tau load in the CNS has been shown to correlate with neuronal loss and with cognitive decline, and may well be the pathological feature of AD that is most closely linked to clinical symptoms [7–9].

Diagnosis of the tauopathies in clinical practice remains challenging, particularly in the earliest stages, and a definite diagnosis in non-genetic cases is only possible with histopathological confirmation, usually only available at autopsy. It would therefore be very valuable to be able to

assess, *in vivo*, the extent and distribution of tau pathology in the brain. With a number of novel diagnostic agents recently developed, quantitative imaging of tau pathology with positron emission tomography (PET) now appears feasible [3]. This advance has significant implications for research and clinical trials, as well as clinical practice, as it could facilitate early and differential diagnosis of the tauopathies, and support measurement of disease progression and assessment of potential disease-modifying treatments.

The PET tracer [^{18}F]AV-1451 (formerly known as [^{18}F]T807) was the first radiotracer reported to have high tau affinity and little cross-reactivity with amyloid-β [10]. Pilot clinical PET scans in AD patients have shown encouraging results suggesting that the tracer might have utility both to diagnose AD and to monitor disease progression [11]. However, further characterisation is needed to determine the potential clinical applications of this PET tracer, particularly for diagnostic imaging of non-AD tauopathies including those in the FTLD spectrum [3,12]. Herein, we report detailed quantification of [^{18}F]AV-1451 binding to *post-mortem* brain tissue from cases with a range of different, well-characterised types of neurodegenerative dementias and control cases.

2. Methods

2.1 Course of the study

Neuropathologically well-characterised cases were selected to cover both a range of different tauopathies and non-tauopathies. The tauopathies were chosen to include cases with predominantly 3R-tau, cases with predominantly 4R-tau and cases with a mixture of 3R- and 4R-tau, namely: Pick's disease (PICK), corticobasal degeneration (CBD), progressive supranuclear palsy (PSP), frontotemporal dementia with parkinsonism linked to chromosome 17 caused by mutations in the microtubule-associated protein tau (MAPT) gene (FTDP-17) as well as AD. The non-tauopathies, included FTLD linked to TAR DNA-binding protein-43 (FTLD-TDP), dementia with Lewy bodies/Parkinson's disease with dementia (DLB/PDD), as well as control cases without brain pathology. Three to six cases per disease group were included, making a total of 33 neurodegenerative dementia cases and four normal control subjects (Table S 1). Two different brain areas per case, always including the frontal cortex, were investigated. The tau load was determined with immunohistochemistry (IHC) in flash frozen brain sections. Phosphorimaging was used to measure the total, specific and non-specific binding of [^{18}F]AV-1451 in adjacent brain sections.

2.2 Case selection

We evaluated tissue from brains donated for research to the Queen Square Brain Bank for Neurological Disorders, Institute of Neurology, University College London. All cases had

undergone standard neuropathological assessment and were diagnosed according to standard criteria. Ethical approval for the study was obtained from the National Hospital for Neurology and Neurosurgery Local Research Ethics Committee.

Normal controls were cases that had died without a history of dementia, psychiatric or neurological diseases. All cases with neurodegenerative diseases had dementia in life (Table 1). The selected AD cases showed “high” AD neuropathological change (CERAD frequent neuritic plaques, Braak and Braak tau stage VI and Thal phase 5 amyloid plaque pathology) using the National Institute on Aging-Alzheimer’s Association guidelines [13-16]. Differential diagnosis of the FTLD-tau cases was carried out following the criteria described by the consortium for Frontotemporal Lobar Degeneration [17]. The chosen FTDP-17 cases included two with an exon 10+16 mutation, one with a R406W mutation and one with an unknown mutation (genetic testing did not reveal any of the common mutations). Frontal and temporal cortices were examined in the AD, PICK and FTDP-17 cases, which were selected due to the presence of abundant tau deposits in these areas. Frontal cortex and cerebellum were assessed in PSP cases, whilst frontal and parietal cortices were studied in CBD. Four subtypes of FTLD-TDP are described (types A to D) and, following the Mackenzie criteria [18], we examined both

FTLD-TDPA and FTLD-TDPC cases containing subtype-specific TDP-43-positive inclusions. DLB/PDD cases exhibited α-synuclein-positive inclusions in frontal and temporal cortices, in accordance with the pathology described by the DLB consortium [19]. The tissues from cases with FTLD-TDPA, FTLD-TDPC, DLB/PDD and normal controls showed no or very low levels of tau or amyloid pathology (Braak and Braak tau stage 0–III and Thal phase 0–3 staging), *i.e.* were not cases with mixed pathology.

2.3 Neuropathological assessment

Routine neuropathological analysis was carried out according to the Queen Square Brain Bank protocol. Paraffin sections (7 μm) were immunostained using commercially available antibodies to the following proteins: TDP-43 (Abnova, Taipei City, Taiwan; 1:800), α-synuclein (Vector, Peterborough, UK; 1:50), tau (AT8 clone; Autogen Bioclear, Wiltshire, UK; 1:600), RD3 and RD4 (gift from Dr. Rohan de Silva) and Aβ (Dako, UK; 1:100) as previously described [20]. Briefly, IHC for all antibodies required pressure cooker pre-treatment in citrate buffer (pH = 6.0). Endogenous peroxidase activity was blocked with 0.3% H_2O_2 in methanol and non-specific binding with 10% dried milk solution. Tissue sections were incubated with the primary antibodies, followed by biotinylated anti-mouse IgG (1:200, 30 minutes; DAKO) and ABC complex (30

minutes; DAKO). Colour was developed with diaminobenzidine/H_2O_2.

2.4 Tau IHC in flash frozen tissue sections

IHC staining in flash frozen tissue sections with AT8 and AT100 was used for characterisation of tau deposits (Figure 1). Tau staining was carried out on adjacent sections to those used for phosphorimaging. Flash frozen tissue sections were cut at 7 μm, mounted on lysine coated microscope slides and post-fixed in 4% paraformaldehyde for 30 minutes. Endogenous peroxidase activity and non-specific binding were blocked as above. Tissue sections were incubated in either AT8 (Autogen Bioclear, Wiltshire, UK; 1:600) or AT100 (Sigma-Aldrich, UK, 1:200) for one hour at room temperature followed by biotinylated anti-mouse IgG (1:200, 30 minutes; DAKO) and ABC complex (30 minutes; DAKO). Colour was developed with diaminobenzidine/H_2O_2. Counterstaining was carried out by immerging the sections into Mayer's hematoxylin (0.1%; BDH, UK) for 30 seconds and by subsequently washing them under running water for 10 seconds.

2.5 Radiochemistry

The precursor for radiolabelling with [^{18}F]fluoride and the non-labelled reference compound AV-1451 were provided by Avid Radiopharmaceuticals, a wholly owned subsidiary of Eli Lilly (Philadelphia, USA), and the radiosynthesis was carried out as previously reported [21].

[^{18}F]AV-1451, formulated in aqueous sodium phosphate buffer (21 mM, 5 ml, containing 10% ethanol), was obtained with an average specific activity of 30 GBq/μmol and a radiochemical purity of > 98%.

2.6 Phosphorimaging

Thawed sections (10 μm mounted on lysine coated microscope slides) from flash frozen tissue were washed in phosphor buffered saline (PBS) for 15 min and subsequently incubated with a solution of [^{18}F]AV-1451 in PBS for 60 min (1 ml per slide). For determination of the total binding, a solution of [^{18}F]AV-1451 in phosphate buffer was diluted with PBS to a concentration of 2 MBq/ml; for determination of the non-specific binding, a solution of the non-radioactive reference compound AV-1451 in ethanol (3.8 mM) was added to a solution of [^{18}F]AV-1451 in phosphate buffer and diluted with PBS to give a final AV-1451 concentration of 2500 × K_d (36.5 μM) and a final [^{18}F]AV-1451 concentration of 2 MBq/ml. After incubation, unbound [^{18}F]AV-1451 was removed by washing the sections in PBS (1 min), 70% ethanol/PBS (2 min), 30% ethanol/PBS (1 min), PBS (1 min) and water (1 min) [10]. Internal standards were prepared by serial dilution of the [^{18}F]AV-1451 solution that was used for the incubation of the brain sections. Brain sections and internal standards absorbed on filter paper were left to air-dry and subsequently exposed to a phosphor screen (BAS-IP MS, GE Healthcare) overnight.

Phosphorimaging was performed on a Typhoon Trio scanner (GE Healthcare).

2.7 Data analysis

Image quantification was performed using the analysis software ImageJ (version 1.48) [22]. Tau load, as detected by AT8 staining in flash frozen tissue, was quantified as % stained tissue detected in the whole brain section. Phosphorimaging experiments were performed in three to six cases per disease group, and at least three adjacent brain sections per case and brain area. Quantification of total and non-specific [^{18}F]AV-1451 binding (mean ± standard deviation in kBq/cm^2) was based on correlation curves generated from the internal standards. Statistical analysis was performed using the software package IBM SPSS Statistics (version 22). The Mann-Whitney U test was used to compare specific binding in disease cases and controls, whereas total and non-specific binding were compared with paired sample t-tests.

3. Results

In AD, a high load of neurofibrillary tangles (NFTs) and neuropil threads was detected in the grey matter, whereas the white matter showed a small amount of threads (Figure 1). PICK cases exhibited Pick's bodies in the grey matter and a dense network of threads in the white matter. Cases with CBD had astrocytic plaques and neuropil threads in the grey matter

and a high load of threads in the white matter. In PSP cases, tufted astrocytes, NFTs and neuropil threads were found in the grey matter, whereas the white matter contained several coiled bodies. NFTs and threads were detected in the grey matter of FTDP-17 cases, whereas the white matter showed long neuropil threads. No tau aggregates were observed in the investigated sections of cases with non-tauopathies, FTLD-TDPA/C and DLB/PDD, or in controls. IHC staining with antibodies specific for 3R- and 4R-tau isoforms [23] confirmed that tau aggregates in AD cases contained a mixture of both isoform subtypes, whereas the inclusion bodies in the PICK cases were, as expected, exclusively formed of 3R-tau and aggregates in the CBD and PSP cases were formed of 4R-tau. The inclusions were exclusively composed of 4R-tau in three of the FTDP-17 cases (two with a confirmed exon 10+16 mutation, one with an unknown mutation) while, in the case with the R406W mutation, as in AD, the inclusions were formed of both 3R- and 4R-tau. In AT8 stained sections, the average tau load in frontal cortices was found to be highest in AD cases (3.0%), followed by CBD (1.1%), PSP (0.9%), PICK (0.8%) and FTDP-17 (0.5%) cases. A comparable tau load was detected in the respective second brain areas that were investigated (Table S 2). Staining with AT100 gave similar results as for AT8.

Excellent morphological correspondence was observed between the tissue sections used for phosphorimaging and those

used for IHC (Figure 2), and visually, there was high consistency between IHC staining of tau and [^{18}F]AV-1451 binding in the AD, PICK, and FTDP-17 cases (Figure 2). In AD, the tracer binding was predominantly in the grey matter, with the global grey-to-white matter ratios ranging from two to four. The specific binding (mean ±standard deviation) in both frontal and temporal lobes (3.4 ±0.9 and 4.2 ±0.5 kBq/cm^2, respectively) was significantly higher ($p < 0.05$) than in the control cases (1.1 ±0.4 and 1.1 ±0.3 kBq/cm^2, respectively) (Figure 3). For the PICK cases, phosphorimaging showed diffuse bands with elevated total [^{18}F]AV-1451 binding that superimposed with the areas stained with AT8. The specific binding was moderate (2.0 ±0.5 and 1.7 ±0.5 kBq/cm^2 in the frontal and temporal cortex, respectively), but still significantly higher ($p < 0.05$) than for controls (1.1 ±0.4 kBq/cm^2). The specific binding to the FTDP-17 cases was comparable to that seen for the PICK cases, and the uptake was similar in both frontal and temporal cortices (average specific binding of 2.1 ±0.7 and 2.1 ±0.8 kBq/cm^2, respectively) for the case with a mixture of 3R- and 4R-tau, and two out of three cases with pure 4R-tau deposits. However, for one of the two cases with a 10+16 MAPT mutation the specific binding was as low as that observed for control cases. Relative to the AD cases, there was a reduced grey-to-white matter contrast for the PICK and FTDP-17 cases, which is in agreement with the IHC evidence

of tau deposition in the white as well as grey matter for these cases. The specific binding of [^{18}F]AV-1451 in the cases with CBD and PSP was low in the brain areas investigated, and not significantly different to that observed for controls. There was no evidence of elevated specific binding in the cases with DLB/PDD, and the mean specific binding in the cases with FTLD-TDP was not statistically different from controls. However, one case with FTLD-TDP type A and one of the cases with FTLD-TDP type C showed elevated specific binding in the frontal cortex.

Significant displaceable binding was observed in all cases, including in non-tau proteinopathies and also in the normal controls ($p < 0.05$). The highest specific binding was observed in AD (73% and 76% of total binding in frontal and temporal cortex, respectively) and FTDP-17 (71% and 70% of total binding in frontal and temporal cortex, respectively). In all other cases, the specific binding, when expressed as percentage of total binding, was comparable to that of control cases (65% and 66% of total binding in the frontal and temporal cortex, respectively).

4. Discussion

In AD cases, a strong, localised and specific signal was obtained confirming that [^{18}F]AV-1451 clearly differentiates AD from control brain tissue. Visually, there was a high degree

of overlap between tracer binding and IHC staining of tau aggregates in AD, as well as PICK and FTDP-17; however, subtle differences were observed, e.g. the layer profile of [^{18}F]AV-1451 in the AD case shown in Figure 2 was not apparent with AT8 staining in the adjacent section. Unexpectedly, with the quantitative analysis we did not find a significant correlation between specific tracer binding and total tau load (% stained tissue area) as determined by IHC with the tau selective antibodies AT8 (Figure 4 and Figure S1) and AT100 [24] in AD tissue, or in any of the other disease groups investigated. However, a weak correlation was found when all cases with tauopathies were included in the analysis (R^2 of 0.24). This is at variance with previous studies which have reported a good correlation of [^{18}F]AV-1451 with tau load in cases with AD [11].

To assess the selectivity of [^{18}F]AV-1451 for tau over other proteins, we investigated the binding to FTLD-TDP type A and type C, DLB/PDD and control cases. No overlap between IHC staining with TDP- and α-synuclein-specific antibodies and [^{18}F]AV-1451 binding was evident; however, for all the above cases low, but significant ($p < 0.05$), displaceable binding was observed (range of 0.7 ±0.2 for DLB/PDD to 1.4 ±0.5 kBq/cm^2 for FTLD-TDP type C), which was comparable to the levels seen for the PSP and CBD cases (0.8 ±0.5 kBq/cm^2). This provides evidence for a non-tau binding site that is unrelated to

pathological changes, and which may affect reliable quantification of tau load with [^{18}F]AV-1451. As tracer binding in *post-mortem* tissue cannot directly be extrapolated to PET imaging, it will be important to determine the degree to which the off-target binding influences the regional brain uptake of [^{18}F]AV-1451 *in vivo*.

Interestingly, the specific binding observed for PICK cases, for which the tau inclusions consist exclusively of 3R-tau, was comparable to that found in two FTDP-17 cases with aggregates formed exclusively of 4R-tau, and one case with mixed 3R-/4R-tau (Table 1), *i.e.* elevated specific binding was not limited simply to tissue expressing either 3R- or 4R-tau. However, it should be noted that the blocking studies were carried out using non-radioactive AV-1451, and hence do not prove that the binding is specific to tau aggregates. Also, the binding to one FTDP-17 case with pure 4R-tau was considerably lower and within the range of controls; further study is required to understand these differences in binding. Relative to the AD cases, for which the global grey-to-white matter ratios were in the range of two to four (specific binding of 3.4 ±0.9 kBq/cm^2 in frontal cortex), the PICK and FTDP-17 cases demonstrated lower specific binding (2.0 ±0.5 kBq/cm^2 and 2.1 ±0.7 kBq/cm^2, respectively) and reduced contrast between grey and white matter. The increased non-specific binding in AD (1.3 ±0.4 kBq/cm^2 in frontal cortex) and PICK

cases (1.1 ±0.3 kBq/cm^2) when compared to controls (0.6 ±0.1 kBq/cm2) indicates that blocking was not complete in the former cases despite using a high concentration (2500 x K_d) of non-radioactive AV-1451. A higher blocking concentration may therefore give an increase in specific binding [25,26].

The finding that there was no elevated [^{18}F]AV-1451 specific binding in PSP and CBD, both pure 4R-tau disorders, but in two out of three FTDP-17 cases in which the tau inclusions were also exclusively composed of 4R-tau, is intriguing and suggests a lack of binding to certain 4R-tau aggregates. As the specific binding of [^{18}F]AV-1451 in the cerebellum of PSP cases and in the parietal cortex of CBD cases was comparable to that observed in the respective frontal cortices, it is unlikely that the low uptake is due to neuronal loss [27,28]. It is, however, possible that [^{18}F]AV-1451 binding is dependent on the tau 'strain', which is characteristic for each disease [29], but further in depth investigations are required to prove this hypothesis. It should be noted that, while the tracer delineated brain regions in the frontal cortex with increased tau load in some of the PSP cases (as determined by IHC), the total binding was still within the range seen for controls. The results imply that although there may be a tau binding site for [^{18}F]AV-1451 in PSP cases, the density of binding sites might be too low for imaging *in vivo*, or the morphology of PSP-tau differs from AD-tau and hence, the affinity of the tracer to PSP-

tau might be lower. This suggests that [^{18}F]AV-1451 is unlikely to be suitable for imaging of tau load in PSP. However, further studies are required to confirm this finding as tracer binding may vary across brain regions. For instance, the midbrain was not examined in this study; if *in vivo* [^{18}F]AV-1451 imaging did reveal tau in the midbrain, then that would be diagnostically useful even if binding to other regions was suboptimal.

In conclusion, the differential binding profile observed suggests that [^{18}F]AV-1451 can be used to qualitatively delineate AD, PICK, and potentially FTDP-17 patients, from healthy subjects, and that grey to white matter ratios may be exploited to differentiate AD from non-AD tauopathies. However, evidence of off-target binding and the lack of correlation between specific binding and IHC staining of tau within the tauopathies investigated, suggest that quantification of tau load *in vivo* with [^{18}F]AV-1451 is likely to be problematic.

Acknowledgements

We thank Avid Radiopharmaceuticals Inc. for providing labelling precursors and methods for the radiosynthesis of [^{18}F]AV-1451. We acknowledge funding by the Leonard Wolfson Experimental Neurology Centre (KS, PG), Alzheimer's Research UK (TL), UCL Business (TG) and the NIHR Queen Square Dementia Biomedical Research Unit. This work was undertaken at UCLH/UCL, which is funded in part

by the Department of Health's NIHR Biomedical Research Centres funding scheme.

Supplementary Data

Supplementary data related to this article can be found at … .

References

[1] Spillantini MG, Goedert M. Tau pathology and neurodegeneration. *Lancet Neurol* **2013**, *12*, (6), 609-622.

[2] Seelaar H, Rohrer JD, Pijnenburg YA, Fox NC, van Swieten JC. Clinical, genetic and pathological heterogeneity of frontotemporal dementia: a review. *J Neurol Neurosurg Psychiatry* **2011**, *82*, (5), 476-486.

[3] Villemagne VL, Okamura N. In vivo tau imaging: obstacles and progress. *Alzheimers Dement* **2014**, *10*, (3 Suppl), S254-264.

[4] Warren JD, Rohrer JD, Rossor MN. Clinical review. Frontotemporal dementia. *BMJ* **2013**, *347*, f4827.

[5] Cairns NJ, Bigio EH, Mackenzie IR, Neumann M, Lee VM, Hatanpaa KJ, White CL, 3rd, Schneider JA, Grinberg LT, Halliday G, Duyckaerts C, Lowe JS, Holm IE, Tolnay M, Okamoto K, Yokoo H, Murayama S, Woulfe J, Munoz DG, Dickson DW, Ince PG, Trojanowski JQ, Mann DM, Consortium for Frontotemporal Lobar D. Neuropathologic diagnostic and nosologic criteria for frontotemporal lobar degeneration: consensus of the Consortium for Frontotemporal Lobar Degeneration. *Acta Neuropathol* **2007**, *114*, (1), 5-22.

[6] Noble W, Hanger DP, Miller CC, Lovestone S. The importance of tau phosphorylation for neurodegenerative diseases. *Front Neurol* **2013**, *4*, 83.

[7] Abner EL, Kryscio RJ, Schmitt FA, Santacruz KS, Jicha GA, Lin Y, Neltner JM, Smith CD, Van Eldik LJ, Nelson PT. "End-stage" neurofibrillary tangle pathology in preclinical Alzheimer's disease: fact or fiction? *J Alzheimers Dis* **2011**, *25*, (3), 445-453.

[8] Arriagada PV, Growdon JH, Hedley-Whyte ET, Hyman BT. Neurofibrillary tangles but not senile plaques parallel duration and severity of Alzheimer's disease. *Neurology* **1992**, *42*, (3), 631-639.

[9] Ossenkoppele R, Schonhaut DR, Baker SL, O'Neil JP, Janabi M, Ghosh PM, Santos M, Miller ZA, Bettcher BM, Gorno-Tempini ML, Miller BL, Jagust WJ, Rabinovici GD. Tau, amyloid, and hypometabolism in a patient with posterior cortical atrophy. *Annals of Neurology* **2015**, *77*, (2), 338-342.

[10] Xia CF, Arteaga J, Chen G, Gangadharmath U, Gomez LF, Kasi D, Lam C, Liang Q, Liu C, Mocharla VP, Mu F, Sinha A, Su H, Szardenings AK, Walsh JC, Wang E, Yu C, Zhang W, Zhao T, Kolb HC. [^{18}F]T807, a novel tau positron emission tomography imaging agent for Alzheimer's disease. *Alzheimers Dement* **2013**, *9*, (6), 666-676.

[11] Chien DT, Szardenings AK, Bahri S, Walsh JC, Mu F, Xia C, Shankle WR, Lerner AJ, Su MY, Elizarov A, Kolb HC. Early clinical PET imaging results with the

novel PHF-tau radioligand [F18]-T808. *J Alzheimers Dis* **2012**, *38*, (1), 171-184.

[12] Shah M, Catafau AM. Molecular Imaging Insights into Neurodegeneration: Focus on Tau PET Radiotracers. *J Nucl Med* **2014**, *55*, (6), 871-874.

[13] Mirra SS, Heyman A, McKeel D, Sumi SM, Crain BJ, Brownlee LM, Vogel FS, Hughes JP, van Belle G, Berg L. The Consortium to Establish a Registry for Alzheimer's Disease (CERAD). Part II. Standardization of the neuropathologic assessment of Alzheimer's disease. *Neurology* **1991**, *41*, (4), 479-486.

[14] Braak H, Braak E. Neuropathological stageing of Alzheimer-related changes. *Acta Neuropathol* **1991**, *82*, (4), 239-259.

[15] Thal DR, Rueb U, Orantes M, Braak H. Phases of A beta-deposition in the human brain and its relevance for the development of AD. Neurology **2000**, *58*, (12), 1791-1800.

[16] Montine TJ, Phelps CH, Beach TG, Bigio EH, Cairns NJ, Dickson DW, Duyckaerts C, Frosch MP, Masliah E, Mirra SS, Nelson PT, Schneider JA, Thal DR, Trojanowski JQ, Vinters HV, Hyman BT. National Institute on Aging-Alzheimer's Association guidelines for the neuropathologic assessment of Alzheimer's disease: a

practical approach. *Acta Neuropathol* **2012**, *123*, (1), 1-11.

[17] Dickson DW, Hauw JJ, Agid Y, Litvan I. Progressive supranuclear palsy and corticobasal degeneration; in: Dickson DW, Weller RO (eds). Neurodegeneration: the molecular pathology of dementia and movement disorders. *Wiley-Blackwell*, *City*, **2011**, pp 135-155.

[18] Mackenzie IR, Neumann M, Baborie A, Sampathu DM, Du Plessis D, Jaros E, Perry RH, Trojanowski JQ, Mann DM, Lee VM. A harmonized classification system for FTLD-TDP pathology. *Acta Neuropathol* **2011**, *122*, (1), 111-113.

[19] McKeith IG, Dickson DW, Lowe J, Emre M, O'Brien JT, Feldman H, Cummings J, Duda JE, Lippa C, Perry EK, Aarsland D, Arai H, Ballard CG, Boeve B, Burn DJ, Costa D, Del Ser T, Dubois B, Galasko D, Gauthier S, Goetz CG, Gomez-Tortosa E, Halliday G, Hansen LA, Hardy J, Iwatsubo T, Kalaria RN, Kaufer D, Kenny RA, Korczyn A, Kosaka K, Lee VM, Lees A, Litvan I, Londos E, Lopez OL, Minoshima S, Mizuno Y, Molina JA, Mukaetova-Ladinska EB, Pasquier F, Perry RH, Schulz JB, Trojanowski JQ, Yamada M, Consortium on DLB. Diagnosis and management of dementia with Lewy bodies: third report of the DLB Consortium. *Neurology* **2005**, *65*, (12), 1863-1872.

[20] Lashley T, Rohrer JD, Bandopadhyay R, Fry C, Ahmed Z, Isaacs AM, Brelstaff JH, Borroni B, Warren JD, Troakes C, King A, Al-Saraj S, Newcombe J, Quinn N, Ostergaard K, Schroder HD, Bojsen-Moller M, Braendgaard H, Fox NC, Rossor MN, Lees AJ, Holton JL, Revesz T. A comparative clinical, pathological, biochemical and genetic study of fused in sarcoma proteinopathies. *Brain* **2011**, *134*, (Pt 9), 2548-2564.

[21] Xiong H, Hoye AT, Fan KH, Li X, Clemens J, Horchler CL, Lim NC, Attardo G. Facile route to 2-fluoropyridines via 2-pyridyltrialkylammonium salts prepared from pyridine *N*-oxides and application to ^{18}F-labeling. *Org Lett* **2015**, *17*, 3716-3729.

[22] Schneider CA, Rasband WS, Eliceiri KW. NIH Image to ImageJ: 25 years of image analysis. *Nat Meth* **2012**, *9*, (7), 671-675.

[23] de Silva R, Lashley T, Gibb G, Hanger D, Hope A, Reid A, Bandopadhyay R, Utton M, Strand C, Jowett T, Khan N, Anderton B, Wood N, Holton J, Revesz T, Lees A. Pathological inclusion bodies in tauopathies contain distinct complements of tau with three or four microtubule-binding repeat domains as demonstrated by new specific monoclonal antibodies. *Neuropathol Appl Neurobiol* **2003**, *29*, (3), 288-302.

[24] Augustinack JC, Schneider A, Mandelkow EM, Hyman BT. Specific tau phosphorylation sites correlate with severity of neuronal cytopathology in Alzheimer's disease. *Acta Neuropathol* **2002**, *103*, (1), 26-35.

[25] Maruyama M, Shimada H, Suhara T, Shinotoh H, Ji B, Maeda J, Zhang MR, Trojanowski JQ, Lee VMY, Ono M, Masamoto K, Takano H, Sahara N, Iwata N, Okamura N, Furumoto S, Kudo Y, Chang Q, Saido TC, Takashima A, Lewis J, Jang MK, Aoki I, Ito H, Higuchi M. Imaging of tau pathology in a tauopathy mouse model and in Alzheimer patients compared to normal controls. *Neuron* **2013**, *79*, (6), 1094-1108.

[26] Varrone A, Steiger C, Schou M, Takano A, Finnema SJ, Guilloteau D, Gulyás B, Halldin C. In vitro autoradiography and in vivo evaluation in cynomolgus monkey of [^{18}F]FE-PE21, a new dopamine transporter PET radioligand. *Synapse* **2009**, *63*, (10), 871-880.

[27] Kanazawa M, Shimohata T, Toyoshima Y, Tada M, Kakita A, Morita T, Ozawa T, Takahashi H, Nishizawa M. Cerebellar involvement in progressive supranuclear palsy: A clinicopathological study. *Mov Disord* **2009**, *24*, (9), 1312-1318.

[28] Kouri N, Whitwell JL, Josephs KA, Rademakers R, Dickson DW. Corticobasal degeneration: a pathologically

distinct 4R tauopathy. *Nat Rev Neurol* **2011**, *7*, (5), 263-272.

[29] Clavaguera F, Akatsu H, Fraser G, Crowther RA, Frank S, Hench Jr, Probst A, Winkler DT, Reichwald J, Staufenbiel M, Ghetti B, Goedert M, Tolnay M. Brain homogenates from human tauopathies induce tau inclusions in mouse brain. *Proc Nat Acad Sci* **2013**, *110*, (23), 9535-9540.

Figure captions

Figure 1. Tau immunohistochemistry. Representative brain sections from cases with different types of dementia showing typical tau aggregates in tauopathies (A, B) and the absence of tau pathology in non-tauopathies and controls (C). Staining was performed with AT8 (A, C) and AT100 (B) antibodies. The left columns show macroscopic images of a brain section, while the centre and right columns show microscopic images (x20 objective) of grey matter (GM) and white matter (WM), respectively. The FTDP-17 case shown has a R406W mutation.

Figure 2. Comparison of AT8 staining and binding of [^{18}F]AV-1451. Representative images showing IHC staining with AT8 (left) and [^{18}F]AV-1451 binding (centre and right; total (TB) and non-specific (NSB) binding) in the adjacent brain sections taken from frontal cortices of selected cases.

Figure 3. [^{18}F]AV-1451 binding to *post-mortem* brain sections from patients with different proteinopathies and controls. Quantification of the total (closed triangles) and the non-specific (open triangles) binding for each case, as well as the average total (continuous line) and non-specific (dotted line) binding in the respective disease groups. The larger the difference between total and non-specific binding (= specific binding), the more specific is the signal obtained and the more precise does it picture the target, *i.e.* tau load in the brain. Brain areas investigated are A) the frontal cortex and B) the temporal

cortex (AD, PICK, FTDP-17, TDPA/C, DLB/PDD, controls), parietal cortex (CBD) and cerebellum (PSP). Mann-Whitney U tests comparing specific binding of [^{18}F]AV-1451 in a disease group to the controls were performed using the software package IBM SPSS Statistics ($p < 0.05$ indicated by *).

Figure 4. Correlation between the specific binding of [^{18}F]AV-1451 and AT8 staining of tau load in cases with tauopathies. The tauopathies are depicted by different symbols (AD, crosses; PICK, triangles; FTDP-17, open circles; PSP, dashes; CBD, squares). The R^2 value considering all cases was 0.24.

Research in context

1. Systematic review: Whilst PET tracers like [^{18}F]AV-1451 have entered clinical trials for imaging of tau load in patients with AD, less is known about their interaction with protein aggregates other than tau and their diagnostic potential in other dementias. We assessed [^{18}F]AV-1451 binding to *post-mortem* brain tissue from patients with a range of neurodegenerative diseases, tauopathies and non-tauopathies, and healthy controls.
2. Interpretation: [^{18}F]AV-1451 is likely to delineate AD, PICK, and FTDP-17 patients from healthy subjects, and allow differential diagnosis of AD from non-AD tauopathies. However, lack of correlation between [^{18}F]AV-1451 binding and IHC, and evidence for a non-tau binding site, suggests that quantification of tau load is problematic.
3. Future directions: The results highlight the importance of characterising PET tracer binding to different tau strains, and to investigate potential cross-reactivity with binding sites distinct from tau, in order to guide clinical applications and facilitate interpretation of PET scans.

Table 1. Case demographics *

Disease	Number of cases (M/F)	Age at onset	Duration (years)	Pathology (IHC)
AD	5 (3/2)	50–70	10–16	GM: NFTs, neurites, NT WM: coiled bodies, NT
PICK	5 (5/0)	53–70	5–17	GM: Pick bodies, ramified astrocytes, NT WM: NT, oligodendroglia
FTDP-17	4 (5/0)	45–59	4–11	GM: NFTs, NT WM: NT
PSP	6 (2/4)	60–70	6–12	GM: tufted astrocytes, NFTs, NT WM: coiled bodies, NT
CBD	4 (2/2)	57–69	6–10	GM: astrocytic plaques, NT WM: NT
FTLD-TDPA	3 (1/2)	57–62	5–10	Cytoplasmic inclusions, threads
FTLD-TDPC	3 (3/0)	50–64	10–15	Corkscrew-shaped neurites
DLB/PDD	3 (0/3)	57–72	20–26	Lewy bodies, α-synuclein positive neurites
Control cases	4 (2/2)	n.a.	n.a.	No tau immunoreactivity

* ***Abbreviations***: M/F, male/female; IHC, immunohistochemistry; AD, Alzheimer's disease; PICK, Pick's disease; FTDP-17, frontotemporal dementia with parkinsonism linked to chromosome 17 (microtubule-associated protein tau mutation); PSP, progressive supranuclear palsy; CBD, corticobasal degeneration; FTLD-TDPA/C, frontotemporal lobar degeneration linked to TAR DNA-binding protein-43, type A/C; DLB/PDD, dementia with Lewy bodies/Parkinson's disease with dementia; GM, grey matter; WM, white matter; NFTs, neurofibrillary tangles; neuropil threads.

Table 2. [^{18}F]AV-1451 uptake, tau load and pathological characterisation of frontal cortices in cases with tauopathies *

Disease	[^{18}F]AV-1451 Uptake SB (kBq/cm^2)	AT8 IHC Tau Load (%)	Tau Isoforms	Tau Filaments	Tau Morphology
PICK	2.0 ±0.5	0.8	3R	SF	Pick bodies, threads
AD	3.4 ±0.9	3.0	3R + 4R	PHF	NFTs, neuritic plaques, threads
FTDP-17	2.1 ±0.7	0.5	3R + 4R, 4R	TR	NFTs, threads
PSP	0.8 ±0.4	0.9	4R	SF	NFTs, threads, astrocytic plaques, coiled bodies
CBD	0.8 ±0.4	1.1	4R	TR	Threads, astrocytic plaques

* ***Abbreviations***: IHC, immunohistochemistry; 3R/4R, tau isoforms with three or four tandem repeats in their microtubule binding domain, SF, straight filaments; PHF, paired helical filaments; TR, twisted ribbons; NFTs, neurofibrillary tangles.

Figure 1

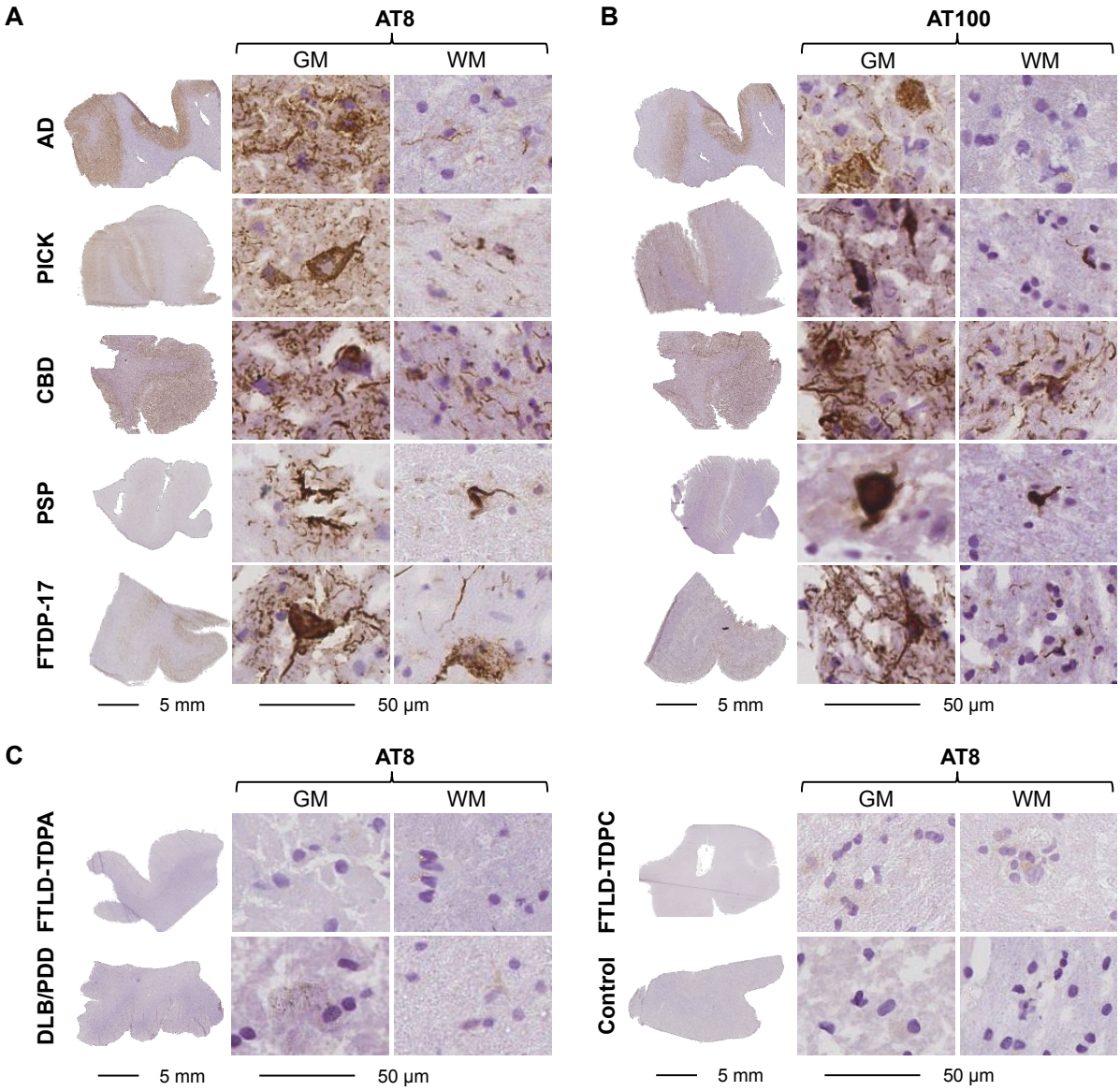
A
AT8
GM
WM
AD
PICK
CBD
PSP
FTDP-17
5 mm
50 µm
B
AT100
GM
WM
5 mm
50 µm
C
AT8
GM
WM
FTLD-TDPA
DLB/PDD
5 mm
50 µm
AT8
GM
WM
FTLD-TDPC
Control
5 mm
50 µm

Figure 2

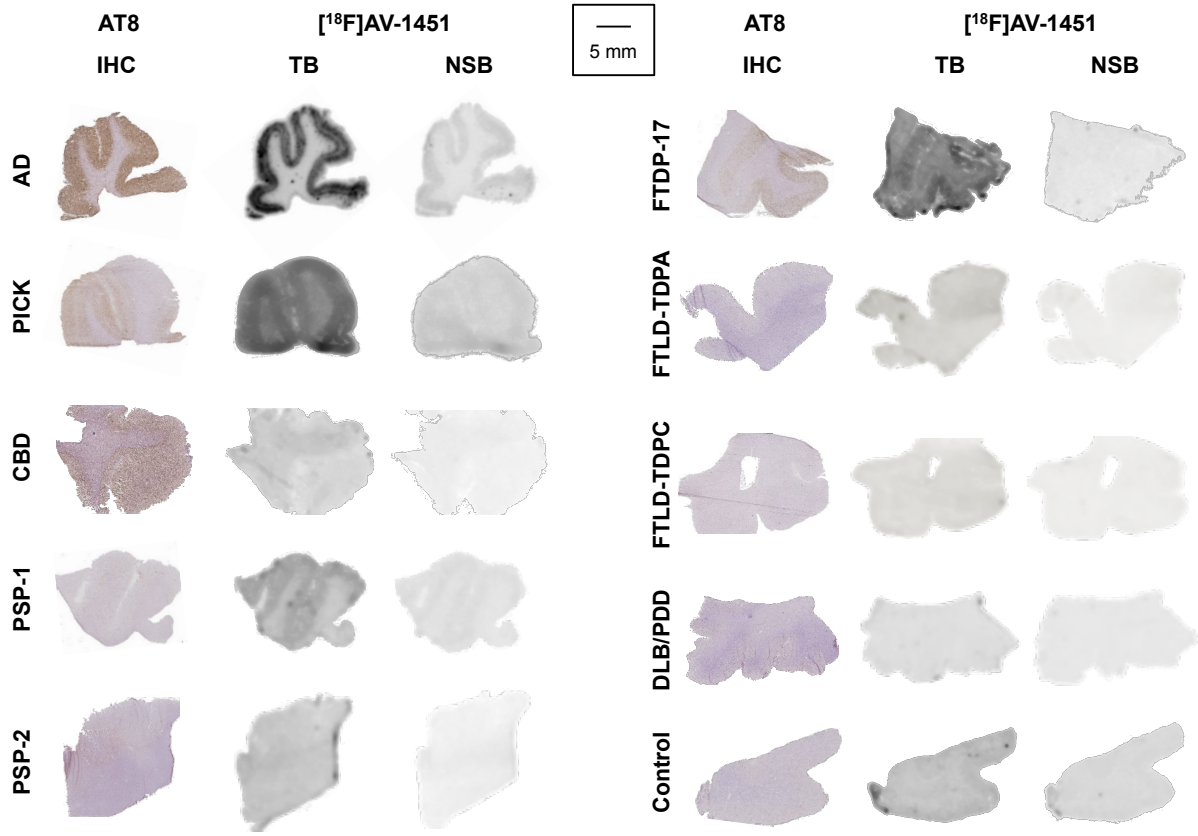
AT8
IHC
[18F]AV-1451
TB
NSB
5 mm
AT8
IHC
[18F]AV-1451
TB
NSB
AD
PICK
CBD
PSP-1
PSP-2
FTDP-17
FTLD-TDPA
FTLD-TDPC
DLB/PDD
Control

Figure 3

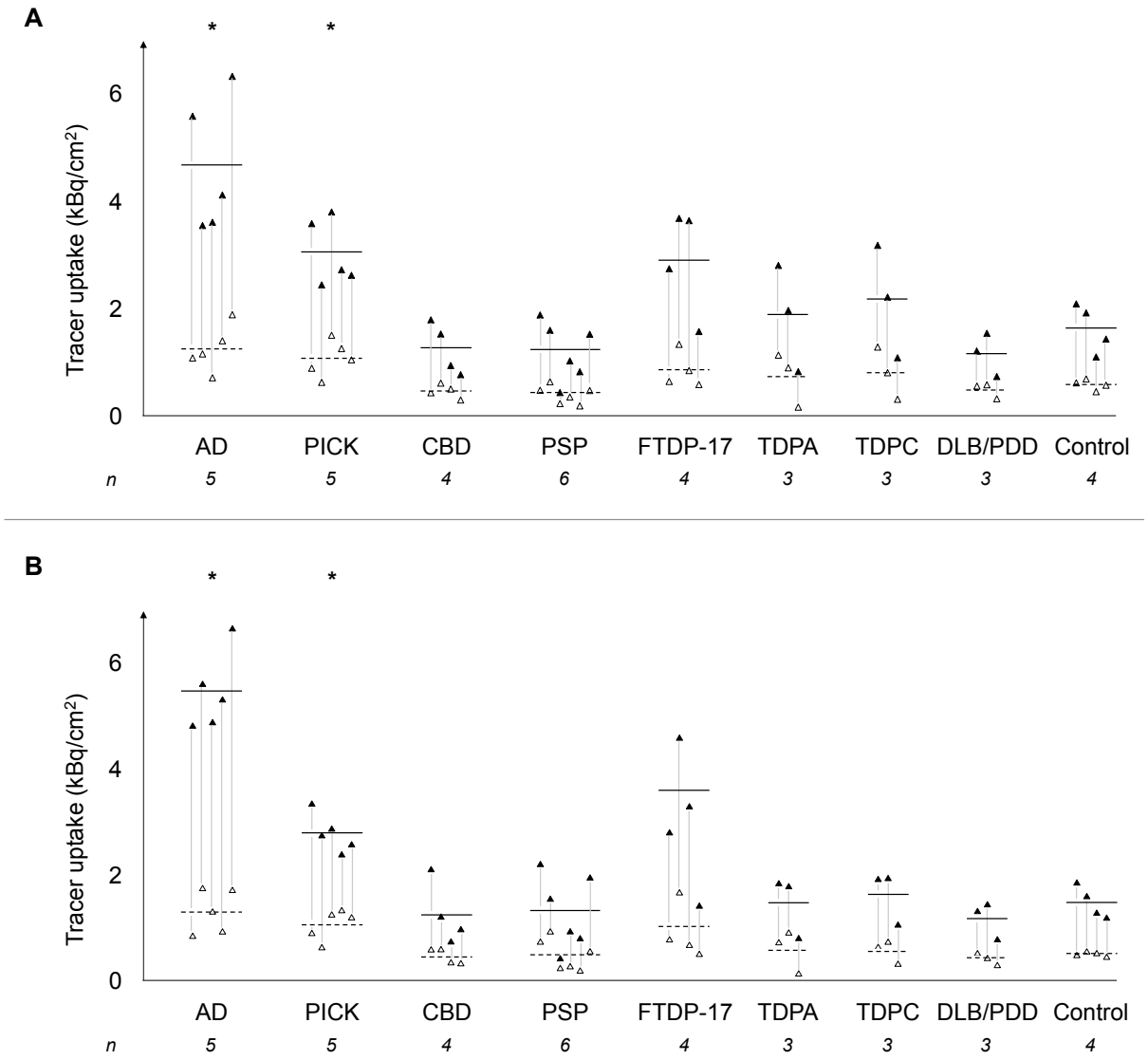
A
*
*
6
4
2
0
Tracer uptake (kBq/cm²)
AD
PICK
CBD
PSP
FTDP-17
TDPA
TDPC
DLB/PDD
Control
n
5
5
4
6
4
3
3
3
4
B
*
*
6
4
2
0
Tracer uptake (kBq/cm²)
AD
PICK
CBD
PSP
FTDP-17
TDPA
TDPC
DLB/PDD
Control
n
5
5
4
6
4
3
3
3
4

Figure 4